Production of Green energy via Water Splitting mechanism by Mn-doped cobalt ferrites [$Co_{1-x}Mn_xFe_2O_4$] based hydroelectric cells

Prachi Jain[a, b], S. Shankar[a], O. P. Thakur [a*]

[a] *Materials Analysis and Research Laboratory, Department of Physics, Netaji Subhas University of Technology, New Delhi 110078, India*
[b] *Functional Materials Research Laboratory, Department of Physics, ARSD College, University of Delhi-110021, India.*

Volume 1, Issue 2, March 2024
Received:11 January, 2024; Accepted: 14 February, 2024
DOI: https://doi.org/10.63015/2h-2419.1.2

**Corresponding author email: opthaku@nsut.ac.in*

Abstract: In our current study, we have investigated the impact of manganese (Mn) doping on the structural, magnetic properties, and hydroelectric cell properties of cobalt ferrite with chemical formula [$Co_{1-x}Mn_xFe_2O_4$, x=0.00, 0.125]. The solid-state approach has been utilized to synthesize the material. XRD measurements revealed the formation of an inverse spinel cubic structure with the space group Fd-3m. FTIR spectra hold a shift in the octahedral and tetrahedral bands with the increase in Mn content in cobalt ferrites. The subsequent rise in ferroelectric behavior has been observed with the net maximum saturation polarization of 1.08μC/cm^2. The variation in the permittivity values has been also studied with the increase in Mn content for dry as well as wet hydroelectric cells. The impedance measurements helped us understand the contribution of grains/grain boundaries in the prepared ferrites. The enhanced value of magnetization has been noticed from 48.258 emu/g to 73.089 emu/g upon doping of Mn ions in cobalt ferrite spinel structure lattice. The Mn doped CFO exhibited enhanced performance in hydroelectric cells which demonstrates the great ionic diffusion mechanism with the incorporation of Mn ions. The obtained output makes Mn doped CFO a suitable material for studying microelectronic and hydroelectric cell applications. The purpose of this study is to enhance both ferroelectric as well as ferromagnetic behavior along with the improved value of current in hydroelectric cells.

Keywords: Ferroelectrics, Multiferroics, Hydroelectric cells, Ferromagnetism, Dielectrics.

1. Introduction: Energy storage has now become a big concern in the society because the consumption of energy is increasing day by day. The evolution of toxic gases by the energy released from fossil fuels is degrading the environment. So, there is a high urge to develop those devices that can generate clean and green energy. The generation of green energy by the hydroelectric cells using a few water droplets has been proven to be a cheap, clean, and eco-friendly technique [1]. Water dissociation has been obtained at room temperature by oxygen-deficient materials without the usage of any electrolytes/ acids/ alkalis, etc [2]. Hydroelectric cells have been already tailored using various metal oxides like TiO_2, SnO_2, MgO, ZnO-CuO, Fe_2O_3, and Al_2O_3 [3-8]. It has been rigorously studied that doping of external elements in ferrite or oxides generates oxygen vacancies in the lattice. Doping of Mg in Al_2O_3 has decreased the internal resistance of oxide and produced the maximum power density of 3.37 mW/cm^2 [9]. A big amount of industrial waste called red mud has been fabricated into a clean and green source of energy (hydroelectric cells) [10].

$CoFe_2O_4$ is an interesting magnetoelectric multiferroic material having a transition temperature (T_C) of ~580K. Its transition temperature can be tuned below or above the room temperature by changing the Fe content in $Fe_{2-x}Mn_xO_4$ (at x =0.125 T_C was 900K) and processing conditions [11]. In contemporary understanding, magnetic materials are classified into various categories, including paramagnetic, diamagnetic, ferromagnetic, ferrimagnetic, antiferromagnetic, super-paramagnetic, and spin glass. Cobalt ferrite nanoparticles have an inverse spinel structure. Co^{2+} and Fe^{3+} occupy either tetrahedral or octahedral interstitial spaces in this O^{2-} form FCC tight packing. Half of the Fe^{3+} ion and Co^{2+} ions are found in the octahedral sites of this inverse spinel cobalt ferrite structure, while the remaining Fe^{3+} ions are found in the tetrahedral sites. Cobalt ferrite features closed-packed spinel arrangements with 32 oxygen ions from unit cells and a secondary phase cubic spinel crystal structure with space group symmetry Fd-3m. The unit cell of the CFO contains a total of 56 atoms. There are 64 tetrahedral sites and 32 octahedral sites in the unit cell containing 32 oxygen ions [12].

It has been observed that Mn doped CFO has decreased the resistance of pure CFO, thereby initiating the fast movement of ions contributing towards improved current [13]. Many findings have been already reported on the storage efficiency of Mn doped CFO. Singh et al. reported the manganese doped ferrite and PANI composite for energy storage electrode material for supercapacitor applications [14]. Milan et al. found increased transport and magnetic properties of CFO upon doping with manganese ion [15]. Fiaz et al. showed the anticancer, antibacterial, and antidiabetic applications of Mn doped CFO [16].

Amongst all available ferrites, the research on manganese (Mn) doped cobalt ferrites (CFO) based hydroelectric cells (HEC) has not been reported yet. Here, we will report the maximum current and voltage produced in Mn doped CFO based HEC.

2. Methodology: The solid-state synthesis route has been followed to prepare the highly porous Mn doped CFO with the chemical composition [$CoFe_2O_4$, $CoMn_{0.125}Fe_{1.875}O_4$] has been shown in Fig 1. The stoichiometric amount of (Co_3O_4, *Loba Chemie*) and (Fe_2O_3, *Fisher Scientific*) were taken and grounded together in an agar pestle mortar in the acetonic medium for 3-4 h constantly. Then, the obtained powder was calcined at 900˚C for 3 h. Obtained calcined powder was further sintered at 50˚C above the calcined temperature for 4 h. Then, the powder was again grounded for 1 h to obtain fine particles.

hydroelectric cells.

Preparation of Hydroelectric cells (HEC): The obtained sample powder was mixed with PVA binder and then transformed into square pellets of dimensions $2\,cm \times 2\,cm$ and thickness of 2mm using a hydraulic presser machine as shown in Fig 2. The square pellets were then hardened by sintering at 250˚C for 2 h to evaporate the PVA binder and to obtain homogeneity in the samples. Silver paint lines were drawn in a comb pattern on one face of all the pellets. A zinc sheet was pasted on the other side of each of the pellets. Finally, electrical contacts were applied to all the pellets to develop them in the form of fully functional HECs.

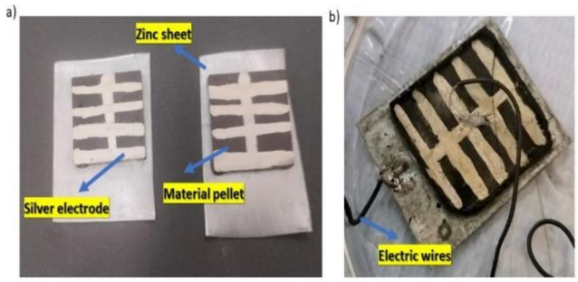

Fig 2. Representation of (a) CFO and (b) Mn-CFO based hydroelectric cells.

3. Characterization Techniques: The XRD measurements of Mn doped CFO were carried out using Bruker D8 Advance X-Ray diffractometer with Cu-K_α radiations (λ= 1.5406Å) in 2θ range extending from 10˚ to

90° with a scanning speed of 1°/min. The FTIR spectra were obtained using Perkin Elmer for measurements in the range of 4100-400 cm^{-1} for solid samples. The surface morphology of the samples was done using the FESEM-EDX Zeiss instrument. Dielectric, Conductivity, and Impedance measurements of all samples were carried out by using a Nova Control Technology Impedance analyzer. The magnetic studies (M-H loop) were recorded using an ADE-EV9 VSM (vibrating sample magnetometer) instrument under a magnetic field of 1 Tesla obtained at room temperature. The V-I measurements of the HEC have been performed using a Keithley 2450 source meter.

4. Results and Discussion

4.1. Morphological analysis: Fig 3. represents the XRD pattern of pure cobalt ferrite (CFO) and manganese doped cobalt ferrites (Mn CFO) recorded using a Panalytical X' Pert Pro MRD diffractometer using Cu K_α radiation (λ= 1.5406Å) obtained at room temperature. The major peaks have been listed as (111), (220), (311), (220), (400), (422), (511), (440), and (533) which are characteristics of a cubic spinel structure with Fd-3m space group. The obtained diffraction peaks are well matched with the standard JCPDS card number: **98-016-0059** for $CoMn_xFe_{2-x}O_4$.[17].

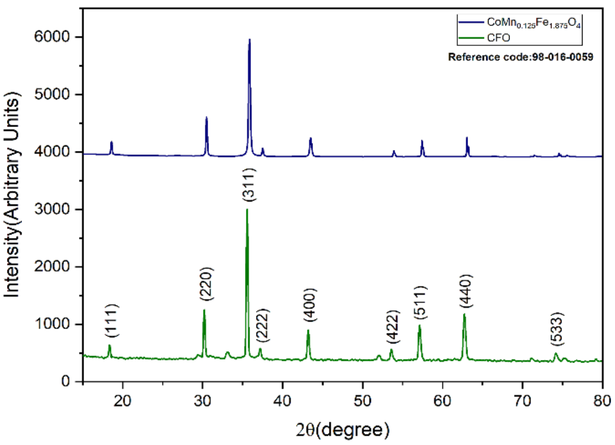

Fig 3. X-ray diffraction data of CFO and $CoMn_{0.125}Fe_{1.875}O_4$ recorded within the 2θ region of 10°-80°; fitted with Fd-3m space group cubic crystal structure.

Table 1 lists the structural parameters that were determined from the XRD pattern, including crystallite size, lattice parameter, interplanar spacing, X-ray density, bulk density, and porosity (%). The formulae for the calculation of these parameters are

Lattice parameter = $d\sqrt{h^2 + k^2 + l^2}$ (1)

X-ray density (D_x) = $\frac{8M}{Na^3}$ (2)

Bulk density (D_b) = Mass of pellet/ Volume of pellet = $m/\Pi r^2 L$ (3)

Porosity (%) = 1- D_b/D_x (4)

Using the W-H plot equation, the average crystallite size (D) and induced microstrain have been calculated as given by equation (5)

$$\beta Cos\theta = (4Sin\theta)\varepsilon + \frac{K\lambda}{D}, \quad (5)$$

where β represents full width at half maximum (FWHM), θ is the angle of strongest intensity peak, ε is the micro-strain, and λ is the wavelength of Cu-Kα (1.54Å) radiation used respectively. The average crystallite size for the prepared MnCFO nanoparticles has been found around 55.69 nm.

It has been observed from Table 1, that the porosity % has increased from 56.75 % to 61.8% with the incorporation of Mn ions in CFO. The doping of foreign dopant atom (Mn) in the pure CFO leads to the formation of defects resulting in a large value of microstrain [18]. The substitution of dopant ions also creates dislocation in the lattice thereby contributing towards the defects. These defects consist of oxygen vacancies which are

Table 1. Useful Parameters calculated from the XRD plots of Manganese doped cobalt ferrites (MnCFO)

Sample	Crystallite size (nm)	Strain ($\times 10^{-3}$)	Lattice parameter (Å)	Volume ($Å^3$)	Interplanar spacing (Å)	Bulk density (g/cm^3)	X-ray density (g/cm^3)	Porosity (%)
$CoFe_2O_4$	51.16	2.13	8.383	589.112	2.527	2.99	4.506	33.644
$CoFe_{2-x}Mn_xO_4$	55.69	0.76	8.385	589.534	2.528	2.91	4.458	34.724

mainly responsible for the interaction of water molecules with the lattice.

4.2.FTIR spectroscopy:

Fourier transform infrared (FTIR) spectroscopy was used to examine the structure and cation distribution between the tetrahedral and octahedral lattice sites in the inverse spinel ferrite, All spinel structures

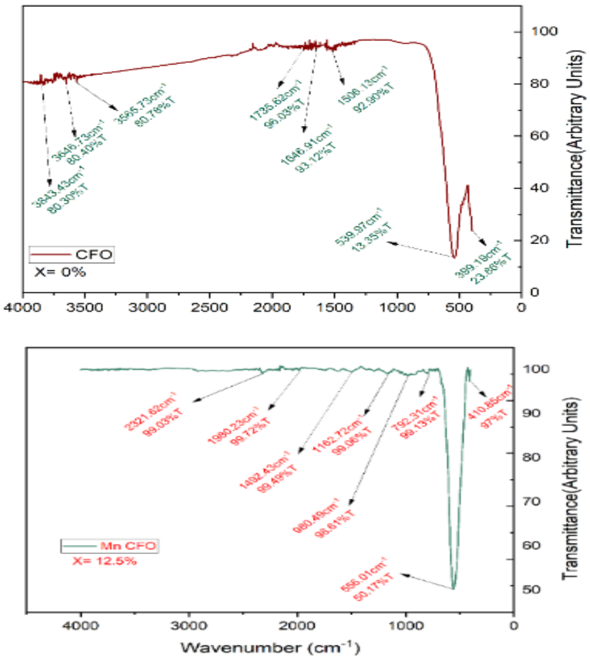

Fig 4. FTIR spectra of (a) CFO (b) Mn-CFO based ferrites.

contain two primary metal-oxygen bands that can be seen in the IR spectrum. Fig 4. shows the FTIR spectrum of pure as well as Mn-doped cobalt ferrite. The band ν_1 for pure and Mn-doped at (539.97 cm^{-1} & 556.01cm^{-1}) arises in the range of 500-600 cm^{-1} due to tetrahedral complexes and ν_2 at 399 cm^{-1} & 410.85 cm^{-1} is due to octahedral complexes [19]. In cobalt ferrite and cobalt ferrite doped with Mn, the O-H bands may be shown to be stretched at a distance of 1506.13 cm^{-1} and bent at a distance of 3843.43 cm^{-1}, respectively. Small particle sizes can cause line broadening and vibrational mode overlap, making it challenging to observe certain bands. The characteristic band ν_1 of spinel ferrites changes to a higher frequency region as the Mn-substitution grows. This is because manganese has a lighter atomic mass than cobalt. Consequently, the frequency of metal-oxygen stretching will rise [20].

4.3.Morphological Studies:

SEM-EDX micrographs of the sintered pellets of $CoFe_2O_4$, $CoMn_{0.125}Fe_{1.875}O_4$ have been recorded at room temperature and are shown in Fig 5. The surface morphology is observed

Table 2. Atomic and weight % obtained for manganese doped cobalt ferrites (Mn-CFO).

Elements	Weight %	Atomic %
O K	21.97	50.07
Mn K	0.65	0.43
Fe K	47.42	30.96
Co K	29.96	18.53

to be quite uniform in both samples. Energy Dispersive X-ray (EDX) micro-analysis is a technique used to determine the elemental composition of a sample. The average grain size of the Mn doped spinel ferrite nanoparticles has been calculated using ImageJ software and found to be near around 69 nm. It provides qualitative information about the presence of different elements like Mn, Co, O, and Fe in the samples and allows for quantitative analysis by determining the

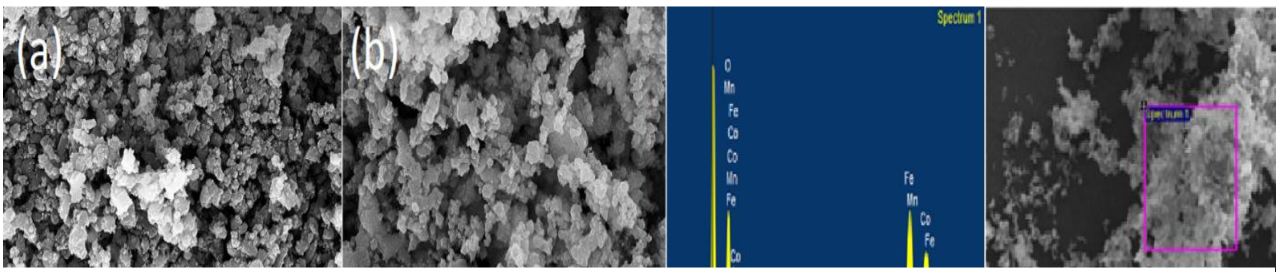

Fig 5. SEM micrograph and compositional study of (a) $CoFe_2O_4$ (b) $CoMn_{0.125}Fe_{1.875}O_4$, sample at 50 k magnification and 20 kV power.

relative abundance or concentration of elements in the sample [21].

4.4. Comparison of Ferroelectricity: Fig 6. exhibits the variation of polarization against the electric field (E=10 KV/cm) for pure as well as Mn doped cobalt ferrites obtained at

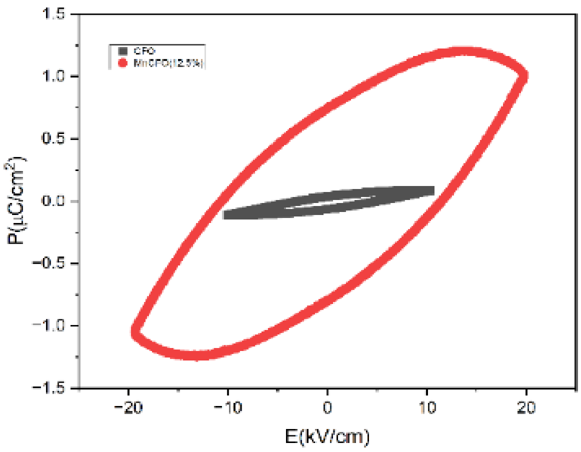

Fig 6. Variation of Polarization (a) $CoFe_2O_4$ (b) $CoMn_{0.125}Fe_{1.875}O_4$, sample with electric field obtained at RT.

room temperature and the applied frequency at 50 Hz. The material appears to be lossy and polycrystalline based on hysteresis loops [22]. It has been observed that the net saturation polarization has been increased to 1.08μC/cm^2 with very small doping of Mn in CFO. The value of net remnant polarization has been also increased upon the addition of Mn in CFO.

4.5. Ferromagnetic Studies: Field-dependent magnetic properties of Mn doped CFO has been shown in Fig 7. as obtained at room temperature. It has been observed that the addition of Mn in CFO caused a vigorous rise in the values of saturation magnetization (M_s) from 48.258 emu/g to 73.089 emu/g. Table 3. exhibits the decrease in coercivity and the subsequent rise in the magnetic properties that occurred for Mn doped CFO. The exclusive rise in the value of M_s is mainly due to the difference in the magnetic moments of the ions present at the A-site and the ions at the B-site. The doping of Mn^{2+} ion caused the replacement of B-site ions and thus altered the magnetic moment of ions present at B-site. Hence, due to the change in the magnetic moment, the net value of (M_s) got intensively increased [23]. The hysteresis loop has occurred at RT showing that material is ferrimagnetic. The magnetic characteristics of

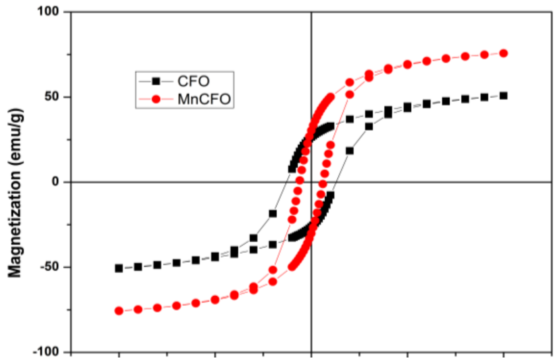

Fig 7. M-H loop of cobalt ferrite & manganese doped (a) $CoFe_2O_4$ (b) $CoMn_{0.125}Fe_{1.875}O_4$, sample cobalt ferrite nanoparticles.

cobalt ferrite nanoparticles are affected by the particle size, production process, and cation dispersion. These elements produce surface disorder brought on by a canted spin structure and random cation distribution. The high surface disorder generally occurs due to the presence of high surface anisotropy [24]. CFO based compounds have been heavily researched because of its strong coercivity, great chemical stability, superior electrical insulation, significant mechanical hardness, and mild saturation magnetization at ambient temperature, etc [25].

Table 3. Values of M_s, M_r, and H_c for manganese doped cobalt ferrites (Mn-CFO)

Chemical compound	M_s (emu/g)	M_r (emu/g)	H_c (Oe)
CFO	48.258	26.502	1266.45
Mn-CFO	73.089	30.490	644.975

4.6. Variation of dielectric constant (ε′) for dry and wet hydroelectric cells: The ability of water dissociation by the Mn doped CFO based HEC and the conduction mechanism has been investigated using an impedance analyzer at room temperature. The variation of dielectric constant against frequency in the frequency range 20 Hz- 10^6

Hz is shown in Fig 8. It has been observed that the dielectric constant (ε′) values has been

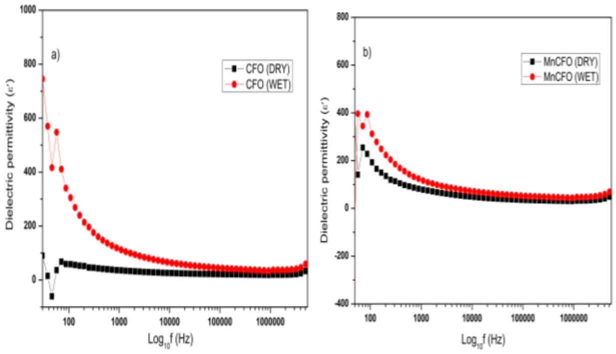

Fig 8. Dielectric constant with frequency for dry and wet hydroelectric cells of (a) $CoFe_2O_4$ (b) $CoMn_{0.125}Fe_{1.875}O_4$.

increased for wet HEC as compared to dry HEC at low frequency range. The ε′ values have become almost constant at high frequency range. This behaviour in the variation of ε′ values is mainly due to rise in ionic and space charge polarization due to dissociated water molecules [26].

4.7. Ionic diffusion Plots: EIS is a highly delicate technique to study the diffusion of ions on the material's surface. The various reactions occurring on the cell surface can be

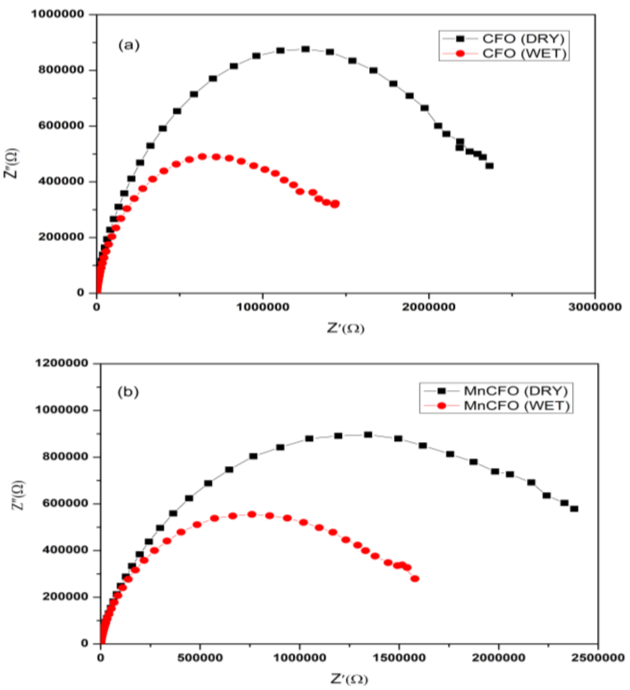

Fig 9. Z′′ vs Z′ plots for dry and wet hydroelectric cells of (a) $CoFe_2O_4$ (b) $CoMn_{0.125}Fe_{1.875}O_4$.

studied using EIS spectroscopy. The Nyquist's plots have shown the large impedance of dry HEC in the order of 107- 108 ohms as compared to wet HEC. Wet HEC exhibit impedance in the range of few kilo ohms. This extreme deduction in the impedance value is due to the dissociation of water molecules into H_3O^+ and OH^- ions. It confirms the water molecules had been adsorbed on the sample surface and got chemidissociated [27].

4.8. Current and voltage studies in Mn doped CFO based hydroelectric cells: The variation of voltage against current for pure cobalt ferrite as well as Mn doped CFO is

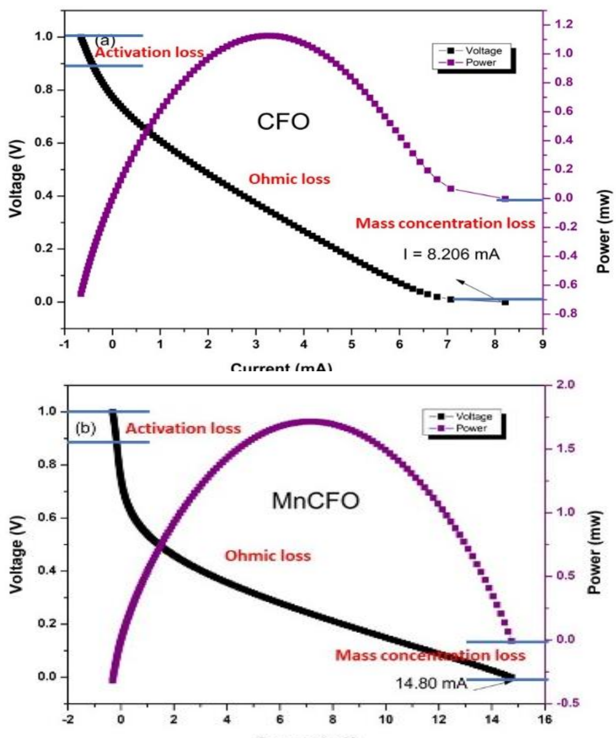

Fig 10. V-I polarization plots for dry and wet HEC of (a) $CoFe_2O_4$ (b) $CoMn_{0.125}Fe_{1.875}O_4$.

shown in Fig 10. The maximum peak off-load current (I_{sc}) around 14.80 mA has been reported for Mn doped CFO based HEC. The high value of current (~ 14.80 mA) has been accommodated due to the production of more oxygen vacancies in Mn doped CFO. It has been observed that the concentration loss gets reduced for doped cells due to which current remains constant for a longer time and gives high value. The whole V-I polarization curve is divided into mainly three regions:- Activation loss, ohmic loss and mass concentration loss. Activation loss refers to the energy barrier for the charge transfer reaction at both electrodes. Ohmic region is the region where voltage decreases in almost linear manner with the current. The sharp degradation in the voltage has been occurred due to the aggregation of ions near the electrodes and caused a concentration loss or mass loss [28,29].

5. Conclusions: A comprehensive investigation was conducted to check the impact of Mn substitution on the generation of current by hydroelectric cells of cobalt ferrites. The presence of Mn^{2+} ions in the lattice has led to the generation of strain and oxygen vacancies. X-ray diffraction pattern and Fourier transform spectroscopy has confirmed the formation of cubic phase of $Co_{1-x}Mn_xFe_2O_4$ (where x = 0.00, 0.125) ferrites. XRD studies revealed the net increment in the porosity % for the Mn doped CFO. Increased porosity initiated increased chemi-dissociation of water molecules. High values of saturation magnetization obtained at room temperature suggests the ferromagnetic nature of the material. The fitted Nyquist plot of Mn doped CFO based HEC shows a drop in both charge transfer resistance and ohmic resistance. This drop, in turn, enhanced the reaction rate and a corresponding enhancement has been observed in ionic conduction. This enhanced ionic conduction produces an output current of 14.80 mA, accompanied by voltage of 0.98 V, for the substitution of Mn in CFO. This study demonstrates the improved performance of hydroelectric cells based on transition metal doped ferrites.

References:

1. Gaur, A., Shah, J., Kotnala, R. K., & Kumar, D. (2022). Development of Mg-doped hematite (α-Fe 2 O 3)-based hydroelectric cell to generate green electricity. *New Journal of Chemistry*, *46*(44), 21158-21166.
2. Manash, A., Singh, R. K., Kumar, V., Shah, J., Das, S. B., Kumar, S. S., ... & Kotnala, R. K. (2023). Studies on structural and magnetic properties of nanoporous Li+ substituted MgFe2O4 nanomaterials for its application in hydroelectric cell with other areas of science & technology. *Materials Today: Proceedings*, *80*, 1002-1013.
3. Bhakar, U., Agarwal, A., Sanghi, S., Shah, J., & Kotnala, R. K. (2021). Production of green electricity from strained BaTiO3 and TiO2 ceramics based hydroelectric cells. *Materials Chemistry and Physics*, *262*, 124277.
4. Kumar, P., Vashishth, S., Sharma, I., & Verma, V. (2021). Porous SnO 2 ceramic-based hydroelectric cells for green power generation. *Journal of Materials Science: Materials in Electronics*, *32*, 1052-1060.
5. Kotnala, R. K., Gupta, R., Shukla, A., Jain, S., Gaur, A., & Shah, J. (2018). Metal oxide based hydroelectric cell for electricity generation by water molecule dissociation without electrolyte/acid. *The Journal of Physical Chemistry C*, *122*(33), 18841-18849.
6. Maurya, I., Gupta, T., Shankar, S., Gaurav, S., Tuli, V., Shah, J., & Kotnala, R. K. (2022). Dielectric and impedance studies of binary ZnO–CuO nanocomposites for hydroelectric cell application. *Materials Chemistry and Physics*, *291*, 126690.
7. Jain, S., Shah, J., Dhakate, S. R., Gupta, G., Sharma, C., & Kotnala, R. K. (2018). Environment-friendly mesoporous magnetite nanoparticles-based hydroelectric cell. *The Journal of Physical Chemistry C*, *122*(11), 5908-5916.
8. Das, R., Shah, J., Sharma, S., Sharma, P. B., & Kotnala, R. K. (2020). Electricity generation by splitting of water from hydroelectric cell: An alternative to solar cell and fuel cell. *International Journal of Energy Research*, *44*(14), 11111-11134.
9. Gupta, R., Shah, J., Das, R., Saini, S., & Kotnala, R. K. (2021). Defect-mediated ionic hopping and green electricity generation in Al 2− x Mg x O 3-based hydroelectric cell. *Journal of Materials Science*, *56*, 1600-1611.
10. Kotnala, R. K., Das, R., Shah, J., Sharma, S., Sharma, C., & Sharma, P. B. (2022). Red mud industrial waste translated into green electricity production by innovating an ingenious process based on

Hydroelectric Cell. *Journal of Environmental Chemical Engineering*, *10*(2), 107299.

11. Yadav, R. S., Kuřitka, I., Vilcakova, J., Havlica, J., Masilko, J., Kalina, L., ... & Hajdúchová, M. (2017). Impact of grain size and structural changes on magnetic, dielectric, electrical, impedance and modulus spectroscopic characteristics of CoFe2O4 nanoparticles synthesized by honey mediated sol-gel combustion method. *Advances in Natural Sciences: Nanoscience and Nanotechnology*, *8*(4), 045002.
12. Thakur, P., Gahlawat, N., Punia, P., Kharbanda, S., Ravelo, B., & Thakur, A. (2022). Cobalt nanoferrites: A review on synthesis, characterization, and applications. *Journal of Superconductivity and Novel Magnetism*, *35*(10), 2639-2669.
13. Kolekar, Y. D., Sanchez, L. J., & Ramana, C. V. (2014). Dielectric relaxations and alternating current conductivity in manganese substituted cobalt ferrite. *Journal of Applied Physics*, *115*(14).
14. Singh, G., & Chandra, S. (2020). Nano-flowered manganese doped ferrite@ PANI composite as energy storage electrode material for supercapacitors. *Journal of Electroanalytical Chemistry*, *874*, 114491.
15. Singh, M., Dubey, B. P., Sahoo, A., Yadav, K. L., & Sharma, Y. (2021). Tailoring the transport and magnetic properties of Mn doped spinel FeCo2O4 and their impact on energy storage properties: A new strategy to improve storage performance. *Journal of Energy Storage*, *44*, 103361.
16. Fiaz, S., Ahmed, M. N., ul Haq, I., Shah, S. W. A., & Waseem, M. (2023). Green synthesis of cobalt ferrite and Mn doped cobalt ferrite nanoparticles: Anticancer, antidiabetic and antibacterial studies. *Journal of Trace Elements in Medicine and Biology*, *80*, 127292.
17. Zawrah, M. F., El-Okr, M. M., Ashery, A., & Abou Hammad, A. B. (2016). Characterization of sol-gel fabricated cobalt ferrite CoFe2O4 nanoparticles. *Middle East Journal of Applied Sciences*, *6*, 362-366.
18. Jain, P., Shankar, S., & Thakur, O. P. (2023). Unveiling the impact of Ni 2+/Y 3+ co-substitution on the structural, dielectric, and impedance properties of multiferroic spinel ferrite for hydroelectric cell application. *Physical Chemistry Chemical Physics*, *25*(32), 21280-21296.
19. Karthickraja, D., Karthi, S., Kumar, G. A., Sardar, D. K., Dannangoda, G. C., Martirosyan, K. S., & Girija, E. K. (2019). Fabrication of core–shell CoFe 2 O 4@ HAp nanoparticles: a novel magnetic platform for biomedical applications. *New Journal of Chemistry*, *43*(34), 13584-13593.
20. Abdel Maksoud, M. I. A., El-Sayyad, G. S., Abd Elkodous, M., & Awed, A. S. (2020). Controllable synthesis of Co1− x M x Fe2O4 nanoparticles (M= Zn, Cu, and Mn; x= 0.0 and 0.5) by cost-effective sol–gel approach: analysis of structure, elastic, thermal, and magnetic properties. *Journal of Materials Science: Materials in Electronics*, *31*(12), 9726-9741.
21. Ashour, A. H., El-Batal, A. I., Maksoud, M. A., El-Sayyad, G. S., Labib, S., Abdeltwab, E., & El-Okr, M. M. (2018). Antimicrobial activity of metal-substituted cobalt ferrite nanoparticles synthesized by sol–gel technique. *Particuology*, *40*, 141-151.
22. Shankar, S., Kumar, M., Ghosh, A. K., Thakur, O. P., & Jayasimhadri, M. (2019). Anomalous ferroelectricity and strong magnetoelectric coupling in CoFe2O4-ferroelectric composites. *Journal of Alloys and Compounds*, *779*, 918-925.
23. Yadav, S. P., Shinde, S. S., Kadam, A. A., & Rajpure, K. Y. (2013). Structural, morphological, dielectrical and magnetic properties of Mn substituted cobalt ferrite. *Journal of Semiconductors*, *34*(9), 093002.
24. Swatsitang, E., Phokha, S., Hunpratub, S., Usher, B., Bootchanont, A., Maensiri, S., & Chindaprasirt, P. (2016). Characterization and magnetic properties of cobalt ferrite nanoparticles. *Journal of Alloys and Compounds*, *664*, 792-797.

25. Rana, K., Thakur, P., Sharma, P., Tomar, M., Gupta, V., & Thakur, A. (2015). Improved structural and magnetic properties of cobalt nanoferrites: influence of sintering temperature. *Ceramics International*, *41*(3), 4492-4497.
26. Jain, P., Shankar, S., & Thakur, O. P. (2022). Dielectric, impedance spectroscopy and hydroelectric phenomena in lanthanum doped bismuth ferrite (Bi0. 85La0. 15FeO3). *Materials Today: Proceedings*, *67*, 742-747.
27. Badola, S., Shah, J., Gaur, A., Khasa, S., Rawal, D. S., Mandal, T. K., ... & Kotnala, R. K. (2023). Strategic enhancement of oxygen defects in ZnO from ZnS for water splitting to generate green electricity by hydroelectric cell. *Applied Materials Today*, *34*, 101904.
28. Gaur, A., Kumar, A., Kumar, P., Agrawal, R., Shah, J., & Kotnala, R. K. (2020). Fabrication of a SnO2-based hydroelectric cell for green energy production. *ACS omega*, *5*(18), 10240-10246.
29. Parray, I. A., Somvanshi, A., & Ali, S. A. (2023). Study of microstructural, ferroelectric and magnetic properties of cerium substituted magnesium ferrite and its potential application as hydroelectric cell. *Ceramics International*, *49*(4), 6946-6957.